

pubs.acs.org/acscatalysis Research Article

Alkane-Soluble Bis[tris(alkylphenyl)carbenium] Diborate Cocatalyst for Olefin Polymerizations

Yanshan Gao, Matthew D. Christianson, Yang Wang, Marc P. Coons, Jiazhen Chen, Jialong Zhang, Steve Marshall, Tracy L. Lohr,* Jerzy Klosin,* and Tobin J. Marks*



Cite This: ACS Catal. 2022, 12, 7589-7597



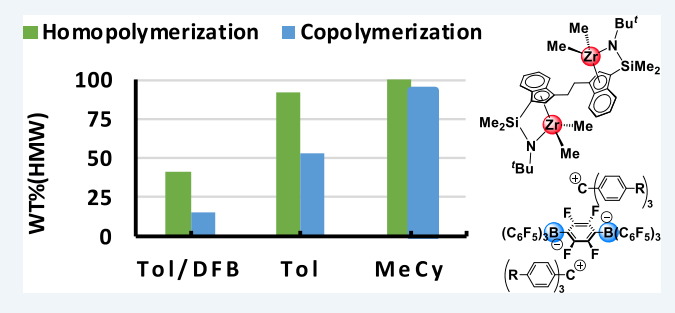
ACCESS

III Metrics & More

Article Recommendations

s Supporting Information

ABSTRACT: Binuclear dianionic cocatalysts can bring cationic active metal centers into close proximity to study center—center enchainment cooperativity effects in olefin polymerization catalysis. The previously reported binuclear diborate cocatalyst, $(Ph_3C^+)_2[1,4-(C_6F_5)_3BC_6F_4B(C_6F_5)_3]^{2-}$ $(\mathbf{B}_{2,\mathrm{H}})$, is poorly soluble in alkane and aromatic solvents and requires undesirable haloaromatic additives to fully solubilize it for efficient olefin polymerizations. Here, two binuclear diborate-based cocatalysts, $(Ar_3C^+)_2[1,4-(C_6F_5)_3BC_6F_4B(C_6F_5)_3]^{2-}$ $(\mathbf{B}_{2,t\text{-Bu}};$ $Ar=4\text{-}t\text{-Bu-}C_6H_4-;$ $\mathbf{B}_{2,n\text{-cotyl}};$ $Ar=4\text{-}n\text{-cotyl-}C_6H_4-)$, are synthesized and characterized by multinuclear NMR spectroscopy, density func-



tional theory computation, and by single-crystal diffraction for $\mathbf{B}_{2,t\text{-Bu}}$. $\mathbf{B}_{2,n\text{-octyl}}$ exhibits good solubility in low-polarity solvents such as toluene and methylcyclohexane (MeCy), enabling the study of $(\mu\text{-CH}_2\text{CH}_2\text{-}3,3')\{(\eta^5\text{-indenyl})[1\text{-Me}_2\text{Si}(^t\text{BuN})](\text{ZrMe}^+)_2$ [EBICGC($(\text{ZrMe}^+)_2$]-catalyzed ethylene homo- and co-polymerizations in solvent systems of decreasing polarity (toluene/difluorobenzene \rightarrow toluene \rightarrow MeCy). Product M_w s are bimodal and sensitive to the above solvent progression, with the high- M_w fraction (wt %) increasing from 41 \rightarrow 92 \rightarrow 100%, respectively, for ethylene homopolymerization, and from 15 \rightarrow 53 \rightarrow 93%, respectively, for ethylene + 1-hexene copolymerization. Under scaled/industrial high temperature, higher pressure operating conditions, the same soluble binuclear diborate is an active olefin copolymerization cocatalyst, giving high polymer M_w s and similar dispersity, D.

KEYWORDS: olefin polymerization, cocatalyst, alkane-soluble cocatalyst, binuclear cocatalyst, enchainment cooperativity

■ INTRODUCTION

Since the pioneering heterogeneous olefin polymerization discoveries of Ziegler and Natta in the 1950s, polyolefins have become some of the most important synthetic materials worldwide. 1,2 More recently, there have been remarkable advances in molecular homogeneous polymerization processes, reflecting extensive breakthroughs in both catalyst and cocatalyst science and technology.³⁻⁵ In contrast to the great proliferation of known organometallic catalysts, there are relatively few cocatalysts^{4–7} of major academic or industrial importance, principally aluminoxanes (MAO and MMAO), 8,9 boranes $[B(C_6F_5)_3]$, and tetrakis(pentafluorophenyl)boratebased ion pairs with triphenylcarbenium (B_{1,H}, Figure 1A) or ammonium countercations. 10-12 These cocatalysts have enabled a broad array of homogeneous polymerization processes, some of which have achieved impressive industrial success. $^{13-18}$ Unfortunately, one limitation of cocatalyst $\mathbf{B}_{1,\mathrm{H}}$ is its insolubility in aliphatic solvents, which are preferred in large-scale processes. Therefore, any potential activity/ selectivity enhancements in aliphatic-only solvents have been largely unattainable with trityl borate derivatives until the recent advent of a more soluble borate cocatalyst [(4-n-octyl $C_6H_4)_3C]^+[B(C_6F_5)_4]^-$ ($B_{1,n-octyl}$). Figure 1A). Here, surprising and informative solvent effects are observed in CGCZrMe₂-catalyzed ethylene polymerizations, including significantly enhanced activity and polyethylene branch densities, as well as altered chain-transfer kinetics.¹⁹

The trityl binuclear diborate cocatalyst, $(Ph_3C^+)_2[1,4-(C_6F_5)_3BC_6F_4B(C_6F_5)_3]^{2-}$ $(\mathbf{B_{2,H}}, Figure\ 1B)$, has been prepared and investigated. Using this diborate dianion as an electrostatic linker can bring two catalytically active cationic metal centers into spatial proximity, enabling binuclearity/cooperativity effects versus the mononuclear analogues in terms of enhanced comonomer enchainment, ethyl branch density, and product stereoselection. $(Ph_3C^+)_2[1,4-(C_6F_5)_3]^{2-1}$

Nevertheless, the widespread use of $B_{2,H}$ -type cocatalysts has been severely limited by the poor solubility in aromatic and

Received: April 6, 2022 Revised: June 1, 2022 Published: June 13, 2022





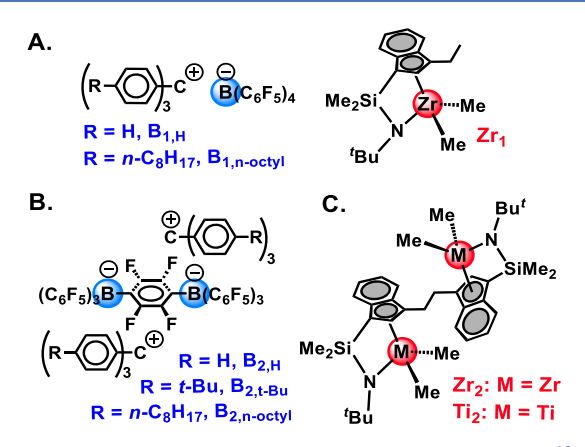


Figure 1. (A) Mononuclear cocatalyst and catalyst structures. ¹⁹ (B) Binuclear cocatalysts and (C) binuclear catalysts existing as diastereomers.

aliphatic solvents, requiring the use of polar haloaromatic additives such as 1,2-difluorobenzene (DFB) to enhance solubility. With very different dielectric constants ($\varepsilon = 13.38$, 2.38, and 2.02 for DFB, toluene, and MeCy, respectively), and basicities as quantified by gas phase proton affinities, the d^0 metal σ - and π -bonding tendencies of these solvents should differ substantially.^{23–25} In view of these limitations, we sought to design and synthesize new soluble binuclear diborate cocatalysts while retaining the robust, charge-dispersing [1,4- $(C_6F_5)_3BC_6F_4B(C_6F_5)_3]^{2-2}$ core. Here, we report that this objective can be achieved by introducing large alkyl substituents on the cocatalyst trityl countercations (Figure 1B). It will be seen here that the new soluble cocatalysts enable polymerizations in additive-free toluene or aliphatic solvents, and that solvent-dependent activity, and wt % high- $M_{\rm w}$ product effects are observed. Under scaled/industrial high temperature, higher pressure operating conditions, the same soluble binuclear diborate is an active olefin copolymerization cocatalyst, giving high polymer $M_{\rm w}$ s and similar dispersity, D.

RESULTS

In presenting our results, we organize the discussion as follows: the synthesis of the hydrocarbon-soluble binuclear cocatalysts is first discussed, followed by single crystal diffraction characterization of the molecular geometry and ion-pairing in $\mathbf{B}_{2,t\text{-Bu}}$. Next, the molecular dynamics of the $\mathbf{B}_{2,t\text{-Bu}}$ and $\mathbf{B}_{2,n\text{-octyl}}$ ion pairs is probed in solution by ^{19}F NMR spectroscopy and by density functional theory (DFT) computation. Finally, ethylene polymerization and ethylene + α -olefin copolymerization experiments are described with the binuclear organozirconium and organotitanium catalysts under both laboratory and industry relevant conditions.

Cocatalyst Synthesis. The synthesis of the new cocatalysts is shown in Scheme 1. Binuclear B₂ cocatalysts are prepared in moderate to good isolated yields (37% for B_{2,t-Bu} and 60% for B_{2,n-octyl}) by salt metathesis of the corresponding trityl chlorides with the known dilithium diborate.²² Both were characterized by ¹H (Figures S4 and S8) and ¹⁹F NMR (Figures S5, S6, and S10-S12), high-resolution mass spectrometry (ESI), and elemental analysis. The goal is to probe catalyst and cocatalyst nuclearity effects in very minimally coordinating solvents, and it is important to assess the conformational dynamics of the weakly coordinating diborate dianion, and thus, we carried out a detailed study of the dianion conformational dynamics using combined single-

Scheme 1. Synthesis of Cocatalysts B_{2,n-octvl} and B_{2,n-octvl}

crystal X-ray diffraction, variable-temperature NMR spectroscopy, and DFT analysis.

Solid-State Structure. Single crystals of $B_{2,t\text{-Bu}}$ suitable for X-ray diffraction analysis were obtained by slow evaporation of toluene/DFB solutions. The basic molecular structure consists of two trityl cations and one dianion (Figure 2). The distances

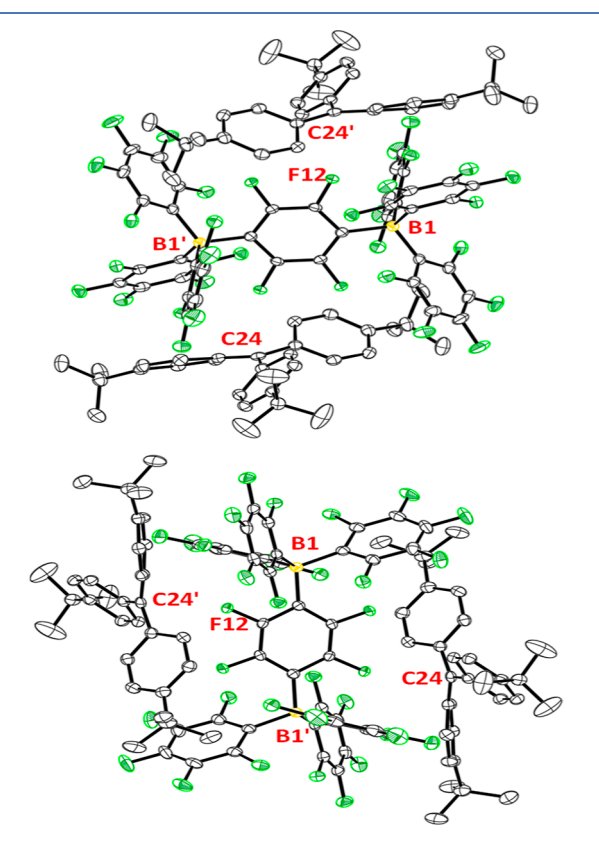


Figure 2. Structure of cocatalyst $B_{2,I\text{-Bu}}$ shown from two perspectives. H atoms are omitted for clarity. Selected atom···atom distances (Å): $B1\cdots B1'=6.211(3),\ B1\cdots C24=7.329(2),\ B1\cdots C24'=5.637(2),\ F12\cdots C24'=3.236(2).$ See Tables S9–S11 for crystal structure details.

between trityl carbon atom C24 (or C24') and boron atoms B1 and B1' (or B1' and B1) are 7.329(2) and 5.637(2) Å (6.483 Å average), respectively, indicating unsymmetrical cation···anion interactions. In comparison, the corresponding average B···C distance in the mononuclear cocatalyst $Ph_3C^+B_-(C_6F_5)_3^-$ is 6.799(6) Å, 26 approximately the average distances of C24 to B1 and B1'. The $B_{2,t\text{-Bu}}$ trityl carbon atoms C24 and C24' are essentially trigonal planar (the sum of bond angles around C24, C24' = 359.8°) and lie roughly above and below the plane defined by the C_6F_4 core. The closest fluorine atom

to C24 is F12 with a F12···C24 distance of 3.236(2) Å. This distance is near the sum of the C and F van der Waals radii, 3.17 Å. 11,27 The B1···B1′ distance is 6.211(3) Å. The approximate B1, B1′ tetrahedral environments are confirmed by all C–B–C angles lying between 112.5 and 113.7° .

Solution Phase Structure—NMR. The two diborate cocatalysts were also characterized by solution ¹H and ¹⁹F NMR spectroscopy, and the multiple resonances for each type of F site (*ortho-*F, *meta-*F, *para-*F, C₆F₄, Figure 3) were

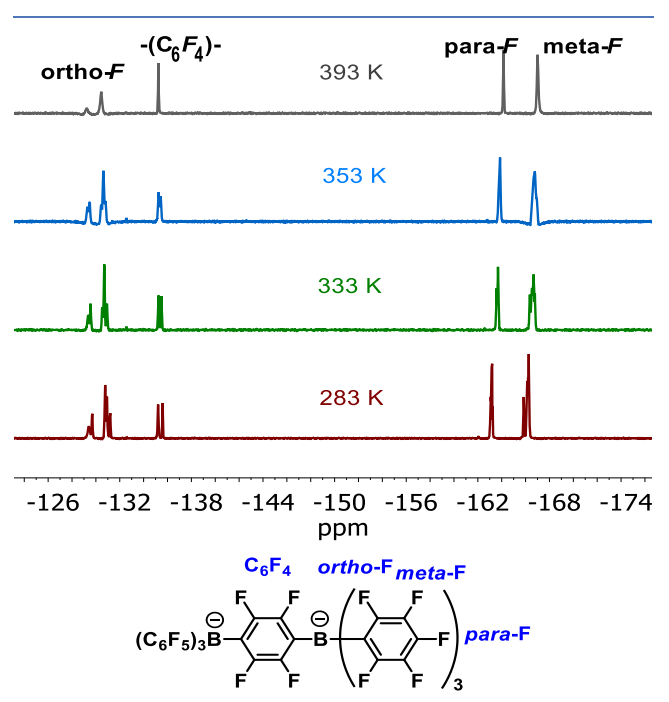


Figure 3. Variable-temperature 470 MHz 19 F NMR spectra of $B_{2\nu_{\text{I-Bu}}}$ in C_6D_5Cl and resonance assignments.

assigned based on the literature. 20-22 Furthermore, 19F EXSY experiments were carried out to probe exchange processes for each type of F site, while solvent and concentration dependence were used to study ion pairing effects. VT 19F NMR was used to study the reversible peak coalescence behavior and approximate free energy barriers for the exchange process in these binuclear cocatalysts. Two resonances for the -C₆F₄- fluorine atoms are found in the ¹⁹F NMR spectrum of B_{2,t-Bu} near room temperature in C₆D₅Cl (Figure 3), which broaden slightly on raising the temperature and then eventually coalesce at highest temperatures. This process is reversible and suggests some combination, perhaps concerted, of hindered rotations about the B-C₆F₅ (see DFT results below) and B-C₆F₄-B axes and/or reorganization of the tight ionpairing. ^{28,29} The free energy barrier for this process, $\Delta G_{363}^{\ddagger}$, is ~18 kcal/mol, estimated from the coalescence temperature of 363 K (Figure 3).^{30,31} A similar coalescence temperature of 376 K is observed for $B_{2,n-octyl}$; however, $B_{2,n-octyl}$ begins to decompose in C₆D₅Cl after prolonged high-temperature

For $B_{2,t-Bu}$, ¹⁹F EXSY NMR spectra in C_6D_5Cl (mixing time = 300 ms) at 50, 60, and 70 °C show exchange between the resonances at δ –135.25 and –135.50 ppm, assigned to the C_6F_4 fragment, as well as exchange between the two multiple peaks at δ –129.20 to –129.66 ppm and –130.43 to –131.04 ppm, assigned to C_6F_5 ortho-F nuclei (Figure S7) are consistent with conformational exchange between nuclei in

the same cocatalyst molecule. Interestingly, the two multiplet peaks belonging to the *ortho*-Fs do not coalesce at temperatures as high as 393 K, whereas the two C_6F_4 peaks coalesce at significantly lower temperature, qualitatively suggesting a higher barrier for $-C_6F_5$ rotation or reorganization. For $\mathbf{B}_{2,n\text{-octyl}}$ ¹⁹F EXSY spectra under the same conditions (Figure S9) also exhibit similar exchange features as observed in $\mathbf{B}_{2,t\text{-Bu}}$. All data confirm that the spectral features belong to the same cocatalyst molecule.

The changes in chemical shifts with temperature may be related to an interplay of steric, solvation, and aggregation ^{19,29,32–34} factors in the ion pairs. Thus, varying the solvent and ion pair concentration was carried out in the ¹⁹F NMR studies of $B_{2,n\text{-octyb}}$ enabled by the good solubility in various solvents. Changing CD₂Cl₂ to C₆D₅Cl, to toluene-d₈, and to cyclohexane-d₁₂ changes the ¹⁹F NMR chemical shifts only slightly (Figure S10), suggesting only minor changes in ion pair aggregation. Furthermore, changing the $B_{2,n\text{-octyl}}$ concentration from 5.75 to 0.34 mM in toluene- d_8 (Figure S11), and from 4.41 to 0.31 mM in cyclohexane-d₁₂ (Figure S12), leads to near-negligible absolute and relative ¹⁹F NMR chemical shift changes, arguing that changes in the ion pair aggregation state 19,29,32 must be relatively minor over this concentration range. Note that the catalyst concentrations for polymerizations are much lower (0.1 mM), so ion pair aggregation is even less likely.19

DFT Analysis. To better understand the structural dynamics of the diborate dianion, relaxed potential energy scans of the B-C₆F₅ torsion of tetrakis(pentafluorophenyl)borate (B_1) and the B1-C₆F₄ torsion of the diborate dianion (B₂) were performed utilizing DFT computation (see the Supporting Information for details). Cartesian coordinates for B_1 and B_2 were obtained from the $B_{1,H}$ and $B_{2,t-Bu}$ crystal structures with the triphenylcarbenium and (4-t-Bu-C₆H₄-)₃C⁺ species removed and served as input for fully relaxed geometry optimizations using both density functionals. The electronic contribution to the relaxed potential energy surfaces was obtained using the \omega B97X-D^{35,36} density functional (Figure 4). Computed surfaces are similar for B₁ and B₂ and are characterized by two unique minimum energy structures, M1 and M2, with electronic energies that differ by <0.1 kcal/mol. For B_1 , the interconversion between M1 and

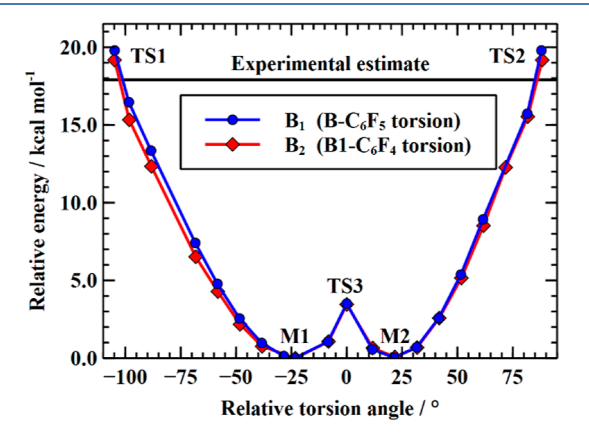


Figure 4. Relaxed potential energy surfaces for rotation of the B– C_6F_5 (B₁) and C_6F_4 –B1′ (B₂) torsions computed with the ω B97X-D density functional (see Figure S3 for comparison to another DFT method). The labels M1–M2 and TS1–TS3 denote locations of fully relaxed minimum energy and transition state structures, respectively.

Table 1. Laboratory-Scale Ethylene Homo- and Copolymerization Data^a

| entry | cocat. | monomer(s) | solvent | yield(g) | act. ^b | $\begin{array}{c} \text{HMW} \\ \text{(kg/mol);} \\ \text{$\text{$\text{$\text{$D$}$}c} \end{array}$ | wt % HMW | LMW (kg/mol); Đ ^c | wt % LMW | ethyl branches/1000 C ^d | <i>n</i> -butyl branches/1000 C ^d |
|-------|---------------------------------|------------|-------------|----------|-------------------|--|------------------|------------------------------|-------------|---------------------------------------|--|
| 1 | $B_{2,H}$ | E | toluene/DFB | 0.21 | 63 | 238; 2.7 | 59 | 3; 2.4 | 41 | 3.6 | 0 |
| 2 | $\mathbf{B}_{2,t	ext{-Bu}}$ | E | toluene/DFB | 0.39 | 118 | 190; 1.8 | 59 | 4; 1.2 | 41 | 4.6 | 0 |
| 3 | $\mathbf{B}_{2,n\text{-octyl}}$ | E | toluene/DFB | 0.46 | 137 | 221; 2.0 | 41 | 2; 1.0 | 59 | 5.7 | 0 |
| 4 | $B_{2,H}$ | E | toluene | 0 | 0 | | | | no activit | y^e | |
| 5 | $\mathbf{B}_{2,t\text{-Bu}}$ | E | toluene | 0 | 0 | | | | no activit | y^e | |
| 6 | $\mathbf{B}_{2,n\text{-octyl}}$ | E | toluene | 0.15 | 45 | 298; 2.3 | 92 | 2; 1.6 | 8 | ~0 | 0 |
| 7 | $\mathbf{B}_{2,\mathrm{H}}$ | E | MeCy | 0 | 0 | | | | no activit | y^e | |
| 8 | $\mathbf{B}_{2,t\text{-Bu}}$ | E | MeCy | 0 | 0 | | | | no activit | y^e | |
| 9 | $\mathbf{B}_{2,n\text{-octyl}}$ | E | MeCy | 0.06 | 18 | 315; 8.5 | 100 ^f | | 0^f | 0.3 | 0 |
| 10 | $\mathbf{B}_{2,n\text{-octyl}}$ | E + H | toluene/DFB | 0.71 | 213 | 96; 2.1 | 15 | 2; 1.0 | 85 | 6.0 | 51.4 |
| 11 | $\mathbf{B}_{2,n\text{-octyl}}$ | E + H | toluene | 0.21 | 64 | 125; 1.9 | 53 | 4; 1.4 | 47 | 3.9 | 57.1 |
| 12 | $\mathbf{B}_{2,n	ext{-octyl}}$ | E + H | MeCy | 0.07 | 21 | 113; 1.9 | 93 | 2; 1.0 | 7 | 0 | 68.2 |

"Conditions: catalyst, $\mathbf{Zr_2}$, 5 μ mol; cocatalyst, $\mathbf{B_2}$, 5 μ mol; solvent for ethylene (E) polymerization, 50 mL of toluene or methylcyclohexane (MeCy), or 48 mL of toluene + 2 mL of DFB (1,2-difluorobenzene); solvent for ethylene (E)/1-hexene (H) copolymerization: 5 mL of 1-hexene; 45 mL of toluene or methylcyclohexane (MeCy), or 43 mL of toluene + 2 mL of DFB; ethylene, 1 atm; temperature, 25 °C, reaction time, 20 min. HMW = high $M_{\rm w}$ fraction; LMW = low $M_{\rm w}$ fraction. Units (kg polymer)·(mol of metal) $^{-1}$ ·h $^{-1}$ ·atm $^{-1}$. GPC vs polystyrene standards in kg·mol $^{-1}$; low- $M_{\rm w}$ samples all have a similar low D pattern, likely reflecting imprecision in calibration. Heavily $^{-1}$ -Arabel density (branches/1000 C) by 13 C NMR. Highly reflects cocatalyst insolubility. Broad D featuring a wide range of $M_{\rm w}$ distribution, including a low $M_{\rm w}$ "tail".

M2 requires concerted rotation of each B-C₆F₅ torsion by 42-45° (see Supporting Information, Tables S5 and S6). Likewise, for B2, interconversion between the two minima proceeds when the $B1-C_6F_4$ and $B1-C_6F_5$ torsions rotate in unison by roughly the same amount as observed for B_1 (see Supporting Information, Tables S7 and S8). Analysis of the transition states at TS3, which are crossed after the rotation of the respective torsions for B_1 and B_2 by $\pm 21-23^{\circ}$ relative to the minimum energy structures, reveal normal modes with vibrational motion indicative of concerted rotation. The electronic energy barrier separating M1 from M2 is found to be 3.2 and 3.5 kcal/mol for B_1 and B_2 , respectively. Thermal corrections to the electronic energies of M1, M2, and TS3 at a temperature of 363 K are found to be ≤1.4 kcal/mol. The resulting free energy of activation for interconversion of M1 into M2 is then 4.3 (B_1) and 4.9 kcal/mol (B_2).

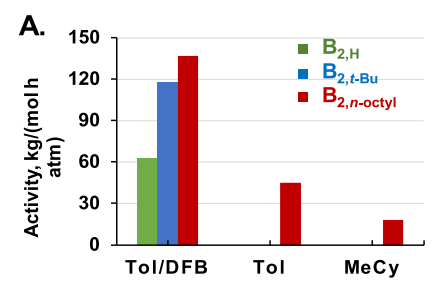
As one B-C₆F₅ torsion of B_1 or the B1-C₆F₄ torsion of B_2 is twisted roughly 80° (65°) away from M1 (M2) and toward TS1 (TS2), each $B-C_6F_5$ or $B1-C_6F_4$ torsion rotates in response by roughly $\pm 10-40^{\circ}$. For B₂, concurrent elongation of the B1···B1' distance by 0.1 Å, half of which arises from lengthening of the C₆F₄-B1' bond, is observed (see Supporting Information, Tables S9 and S10). Furthermore, in an effort to accommodate the C₆F₅ groups that approach the C₆F₄ core during rotation of the B1-C₆F₅ torsion, the two nearest fluorine atoms move away from the plane defined by the carbon atoms of the C₆F₄ core (see Supporting Information, Figure S1). The electronic activation barrier associated with these processes is found to be 19.8 (B_1) and 19.1 kcal/mol (B_2). Thermal corrections to the electronic energies of transition states at TS1 and TS2 at the coalescence temperature of 363 K were ≤1.0 kcal/mol. The computed free energy barrier, $\Delta G_{363}^{\ddagger}$, is found to be 20.2 for B_1 and 20.1 kcal/ mol for B_2 , the latter showing reasonable agreement with the experimental NMR estimate of 17.9 kcal/mol above.

Laboratory-Scale Olefin Polymerizations and Copolymerizations. As noted above, the trityl n-octyl substituents on $B_{2,n\text{-octyl}}$ significantly increase its solubility at 25 °C. Thus, the solubility of $B_{2,n\text{-octyl}}$ is more than 30 mg/mL in both toluene and MeCy (Table S1), sufficient for both laboratory and

larger-scale industrial polymerization catalysis requirements. In contrast, more symmetrical and compact $B_{2,t\text{-Bu}}$ achieves only sparing solubility in toluene or MeCy, comparable to that of $B_{2,H}$. Thus, the excellent solubility of $B_{2,n\text{-octyl}}$ allows for the use of binuclear diborate cocatalyst even in an aliphatic solvent. In contrast, the original binuclear diborate cocatalyst $B_{2,H}$, which can be viewed as a control, is completely insoluble even in toluene, and the catalyst cannot be activated no matter how much toluene or aliphatic solvent is used.

Ethylene polymerization studies using the binuclear catalyst Zr₂ with the soluble diborate cocatalyst were carried out to study solvent effects on polymerization activity, selectivity, and the resulting polyolefin properties. In a previous report, solvent effect studies of polymerizations mediated by the mononuclear analogue, $Zr_1 + B_{1,n-octyl}$ (Figure 1A), were described.¹⁹ The present focus is on binuclearity effects, including solvent effects, for a comparison of both laboratory scale and larger scale polymerization, including a brief comparison/contrast with the solvent effects previously observed for $\mathbf{Zr}_1 + \mathbf{B}_{1,n\text{-octyl}}$. Polymerizations were carried out using rigorously anhydrous and anaerobic methodology with attention to exotherm and mass transfer effects^{38,39} Note in viewing the data that cocatalysts $B_{2,H^{\prime}}$ $B_{2,t\text{-Bu}^{\prime}}$ and $B_{2,\textit{n-octyl}}$ have an identical counteranion and that a small quantity of DFB is necessary to dissolve $B_{2,H}$ and $B_{2,\text{$t$-Bu$}\prime}$ but not $B_{2,\text{$n$-octyl.}}$

For lab-scale $\mathbf{Zr_2} + \mathbf{B_2}$ -catalyzed ethylene polymerizations in toluene/DFB mixture, polymerization activity increases in the order of $\mathbf{B_{2,H}} < \mathbf{B_{2,t\text{-Bu}}} \approx \mathbf{B_{2,n\text{-octyl}}}$, with activities of 63, 118, and 137 (kg polymer)·(mol of metal) $^{-1}\cdot h^{-1}\cdot atm^{-1}$, respectively (Table 1, entries 1–3). When polymerizations are carried out in toluene or MeCy without DFB, neither $\mathbf{B_{2,H}}$ nor $\mathbf{B_{2,t\text{-Bu}}}$ produces catalysts with significant activity (Table 1, entries 4, 5, 7, and 8), presumably due to their poor solubility and therefore lack of reactivity in non-polar solvents. However, $\mathbf{Zr_2} + \mathbf{B_{2,n\text{-octyl}}}$ is active in all cases, although with activity falling as $137 \rightarrow 45 \rightarrow 18$ (kg polymer)·(mol of metal) $^{-1}\cdot h^{-1}\cdot atm^{-1}$ for toluene/DFB \rightarrow toluene \rightarrow MeCy (Table 1, entries 3, 6, and 9; Figure 5A). Note that gel permeation chromatography (GPC) analysis of the PEs obtained from $\mathbf{Zr_2} + \mathbf{B_{2,n\text{-octyl}}}$ in the three solvents show bimodal distributions, dominated by one



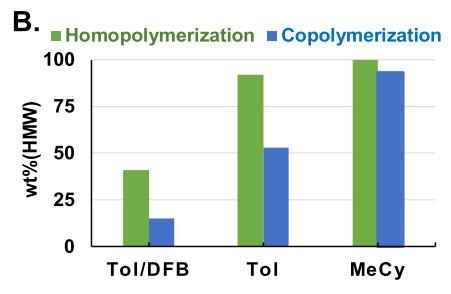


Figure 5. A) Cocatalyst effects on ethylene polymerization activity of $\mathbf{Zr_2} + \mathbf{B_2}$ in various solvents; (B) solvent effects on product wt % (HMW) in $\mathbf{Zr_2} + \mathbf{B_{2,n-octyl}}$ -catalyzed ethylene homo- and 1-hexene copolymerizations. Tol = toluene, DFB = 1,2-difluorobenzene, MeCy = methylcyclohexane.

low-molecular-weight (LMW) fraction and one high-molecular-weight (HMW) fraction (Figures 5B and S23-S30). Note that the wt % LMW falls as the solvent is varied from toluene/ DFB \rightarrow toluene \rightarrow MeCy (Table 1, entries 3, 6, and 9; Figure 5B). Importantly, ¹³C NMR analysis of the bimodal PEs obtained using $Zr_2 + B_{2,n-octyl}$ shows that branch density falls from 5.7 ethyl branches/1000 C to essentially ~0/1000 C as the solvent is changed from toluene/DFB \rightarrow toluene \rightarrow MeCy (Table 1, entries 6 and 9 vs 3). The ethyl branches appear to be localized primarily in the LMW fraction, the percentage of which decreases with the decrease in solvent polarity (see more below). Note that the ¹H NMR spectra of all polymer samples in this study show chain end unsaturation as reported previously, 21,43 suggesting β -H elimination or chain-transfer to monomer is the principal chain termination pathway. The dicationic catalytic species is probably marginally soluble in aliphatic solvents as Zr-CH3+ species. However, note that $B_{2,n\text{-octyl}}$ is very soluble in aliphatic solvents, and that the in situ generated catalytic species is spray-injected into the rapidly stirred olefin solutions to start the polymerization process. It is reasonable that ethylene and 1-hexene coordination and the rapid formation of growing polymer chains at the Zr cationic center help stabilize the species, enhance its solubility, and thus polymerization activity. The polydispersities near 2.0 in Table 1 entries 3, 6, and 12 are in reasonable accord with a normal homogeneous single-site process; the exception is entry 9 which may reflect solubility constraints.

Next, ethylene + 1-hexene copolymerizations using $\mathbb{Z}\mathbf{r}_2$ + $\mathbb{B}_{2,n\text{-octyl}}$ were investigated. There is a minor increase in n-butyl branch density, $51.4 \rightarrow 57.1 \rightarrow 68.2$ n-butyl branches/1000 C, by changing the solvent from toluene/DFB \rightarrow toluene \rightarrow MeCy (Table 1, entries 10, 11, and 12). Interestingly, a progressive fall in ethyl branch density is also observed over this same solvent variation. These polyolefins also have bimodal molecular weight distributions with HMW/LMW ratios affected by the polymerization solvent. Similar to the homopolymerizations discussed above, an increase in HMW

wt % from 15 \rightarrow 53 \rightarrow 93% is observed on solvent variation from toluene/DFB \rightarrow toluene \rightarrow MeCy (Table 1, entries 10, 11, and 12). Note that single-site homogeneous olefin polymerization catalysis usually produces characteristic narrow molecular weight distributions with Φ \sim 2.0. In some scenarios, broadened polyolefin Φ s and multimodality can positively alter melt processing and polyolefin properties.

For the present bimodal HMW + LMW PEs, an intriguing question arises as to whether the branching detected in the mixtures can be described by something as simple as the sum of only two branch types and densities. Thus, a digital ¹³C NMR spectral subtraction analysis was carried out using the samples of Table 1, entries 9 and 3. Polyethylene samples of these entries are either exclusively or partially HMW based on GPC analysis (Figures 5B and S23–S30), with trace branching evident in the ¹³C NMR of the former. Subtracting the ¹³C NMR features of the entry 9 sample from that of entry 3 (Figure S22) yields a spectrum that arguably is near that of the LMW fraction (Table 2). The calculated LMW fraction has

Table 2. Polyethylene ¹³C NMR Spectrum Digital Subtraction Analysis Compared to GPC Analysis ^a

| | wt % (GPC) | wt % (NMR subtraction method) ^b | ethyl branch density, branches/1000 C |
|---------|---------------|--|--|
| HMW | 41 | 45 | ~0.3° |
| LMW | 59 | 55 | 10.1 |
| Mixture | 100 | 100 | 5.7^{c} |

"From digitally subtracting the 13 C NMR spectrum of sample entry 9, Table 1 from that of sample entry 3, Table 1 (Figure S22). b wt % (subtraction) calculated from ethyl branch density of LMW fraction (by 13 C NMR subtraction) and total sample. c Ethyl branch density in branches/1000 C determined by 13 C NMR.

10.1 ethyl branches/1000 C leading to an averaged 5.7 ethyl branches/1000 C for the bulk sample, corresponding to 55 wt % LMW. This result is in good agreement with the 59 wt % LMW determined by GPC analysis.

Larger-Scale Olefin Polymerizations. The above results demonstrate that the soluble $B_{2,n\text{-octyl}}$ cocatalyst enables ethylene homo- and copolymerizations in toluene and even an aliphatic solvent on the laboratory scale. Next, ethylene + 1-octene copolymerizations were investigated using $B_{2,n\text{-octyl}}$ together with Ti_2 and Zr_2 (Figure 1C) under larger-scale conditions relevant to industrial applications. Ethylene + 1-octene copolymerizations were carried out at $120~^{\circ}\text{C}$ in 2 L semi-batch reactors. To load 46 g of ethylene in the reactor, the ethylene pressure was maintained at 18.5 or 18.0 atm with Isopar E (aliphatic solvent similar to MeCy) or toluene as the solvent, respectively. Initial ethylene + 1-octene molar ratio was 1:2.1 in the liquid phase and ethylene was fed on demand to maintain steady concentration during the polymerization reaction.

Solvent effects are again observed in these larger-scale $\mathbf{Zr}_2 + \mathbf{B}_2$ -catalyzed ethylene copolymerizations. On switching the reaction solvent from toluene to aliphatic Isopar E, the polymerization activity is not influenced, while the 1-octene comonomer content increases from 8.7 to 16.5 mol %. The corresponding polymer $M_{\rm w}s$ are 18.5 and 26 kg/mol (Table 3, entries 1 and 2), respectively, and both significantly higher than those at 25 °C (Table 1). As in the above lab-scale experiments, the product dispersity (D) indicates substantial multimodal product formation under these polymerization

Table 3. Large-Scale Ethylene + 1-Octene Copolymerizations at Higher Temperature and Pressure^a

| entry | precatalyst (μ mol) | activator (μ mol) | solvent | polymer (g) | activity ^b | $M_{ m w} \ ({ m g/mol})^c$ | D^c | incorp. (mol %) ^d |
|-------|--------------------------|---------------------------------------|----------|-------------|-----------------------|-----------------------------|-------|------------------------------|
| 1 | $Zr_2(1.0)$ | $\mathbf{B}_{2,n\text{-octyl}}$ (1.0) | toluene | 10.5 | 1,750 | 18,500 | 21.5 | 8.7 |
| 2 | $Zr_2(1.0)$ | $\mathbf{B}_{2,n\text{-octyl}}$ (1.0) | Isopar E | 9.8 | 1,633 | 26,000 | 23.5 | 16.5 |
| 3 | $Ti_2(0.4)$ | $\mathbf{B}_{2,n\text{-octyl}}$ (0.4) | toluene | 10.1 | 4,208 | 117,000 | 7.3 | 18.9 |
| 4 | $Ti_2(0.4)$ | $\mathbf{B}_{2,n\text{-octyl}}$ (0.4) | Isopar E | 12.9 | 5,375 | 112,000 | 6.2 | 25.4 |
| 5 | CGC (0.2) | $\mathbf{B}_{2,n\text{-octyl}}$ (0.2) | Isopar E | 49.0 | 81,667 | 43,000 | 2.4 | 28.5 |
| 6 | CGC (0.2) | $B_{1,H}(0.2)$ | Isopar E | 60.5 | 100,833 | 40,000 | 2.5 | 29.2 |

"Conditions: 2 L batch reactor, cocatalyst, 1.0 equiv $\mathbf{B}_{2,n\text{-octyl}}$; 605 g of Isopar-E, or 691 g of toluene; 295 g of 1-octene in Isopar-E, or 272 g of 1-octene in toluene; 46 g of ethylene loaded (18.5 atm in Isopar-E, or 18.0 atm in toluene); temperature, 120 °C; reaction time, 10 min. ^bUnits (kg polymer)·(mol of metal) $^{-1}$ ·h $^{-1}$ ·atm $^{-1}$. ^cUnits kg/mol; polyethylene equivalent molecular weight by GPC relative to polystyrene standards. ^d1-Octene incorporation in mol % determined by compositional GPC with IR5 detector, end group corrected bulk mol % comonomer; CGC = $\{(\eta^5 - C_5 M_{e_4}) \text{ (SiMe}_2 - N - t - Bu) \text{TiMe}_2; \mathbf{B}_{1,H} = [Ph_3 C]^+[B(C_6 F_5)_4]^- \text{ (Figure 1A)}.$

conditions. Note that these activities in toluene and aliphatic solvent Isopar E are significantly, and not surprisingly, higher than those at 25 °C and 1.0 atm ethylene pressure in Table 1.

Cocatalyst $B_{2,n-\text{octyl}}$ was also used to investigate Ti_2 -mediated ethylene + 1-octene copolymerizations in toluene and Isopar E. Overall, the Ti2 reactions proceed with higher activity and yield higher $M_{\rm w}$ polymers than ${\bf Zr_2}$. Within the ${\bf Ti_2}$ series, there is a slight increase in activity from 4208 to 5375 (kg polymer). (mol of metal)⁻¹·h⁻¹·atm⁻¹ on changing the solvent from toluene to Isopar E, with similar 1-octene incorporations, $M_{\rm w}$ s, and broad Ds. For example, ethylene polymerization using Zr₂ in toluene (entry 1) affords polymer with 75 wt % LMW fraction and 25 wt % HMW fraction; in contrast, polymerization in Isopar-E affords polymer with increased HMW fraction (52 wt %) versus LMW fraction (48 wt %). For comparison, the CGC catalyst was run under the same conditions with both $B_{2,n\text{-octyl}}$ and $B_{1,H}$. As expected, the CGC complex exhibited higher overall activity with activity being very similar for both dinuclear and mononuclear activators. The polymer characterization data indicate single site behavior for both activators and this study indicates that the new soluble binuclear diborate cocatalyst functions well in polymerizations under scaled industrial operating conditions.

DISCUSSION

Bimodal Products. Interestingly, the Ds of the HMW and LMW fractions of most samples are below 2.7, consistent with single-site-like behavior producing each fraction. 48 Earlier work showed that ion-pairing tightness, which is solvent polaritydependent, has a substantial effect on single-site catalyst polymerization rate, comonomer enchainment selectivity, product tacticity, and product polyolefin $M_{\rm w}$. There are two reasonable scenarios that rationalize this intriguing solvent-dependent $M_{\rm w}$ behavior: 52 (1). There are two distinct active sites, one for ethylene oligomerization producing vinylterminated macromonomers, the LMW fraction, and the other for ethylene homopolymerization producing the HMW fraction. The solvent dependence could in principle arise from either differential binding in competition with olefins of the diastereomeric active sites by weakly coordinating solvents, and/or by weakening their ion-pairing to different degrees, and thus leading to solvent-dependent HMW/LMW product ratios. Note that the Zr₂ (and Ti₂) catalysts exist as two NMR-distinguishable but to date inseparable diastereomers (Figure 6A). Once activated with the binuclear cocatalyst, the Zr/Ti diastereomers are expected to form diastereomeric catalytically active species, and these different active species plausibly account for the low and high $M_{\rm w}$ product fractions.

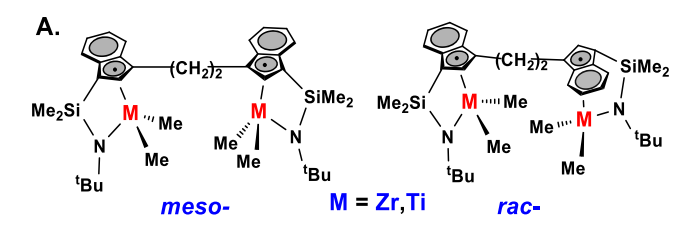




Figure 6. A) Diastereomers of the Ti₂ and Zr₂ precatalysts used in this study. (B) Diastereomers of another series of binuclear group 4 polymerization catalysts.⁵³

Similarly in regard to scenario (1) above, note that different catalytic performance by different catalytic diastereomers was recently reported for a bimetallic constrained geometry Ti catalyst also having rac- and meso-diastereomers (Figure 6B), in that case separable by fractional crystallization. In that example, the two diastereomers demonstrate distinctive and different stereochemically linked cooperative effects on product M_n , tacticity, and comonomer selection.⁵³ (2) Oligomerization at one diastereomer and the resulting vinylterminated macromonomer reinsertion at another would yield HMW and LMW fractions, respectively. The latter case should lead to a HMW fraction with short and long branches (HMW) due to branched macromonomer reinsertion. The negligible branching in the present HMW samples (Table 1, entry 6) indicates the latter scenario is less likely in the current catalyst system. Note that we previously investigated the reaction of $Zr_1 + B_{1,n-octyl}$ by in situ NMR and found facile and complete There is still an additional possible scenario associated with the efficiency of catalyst activation, that is, mono versus doubly activated catalyst(s), for which we have no direct evidence.53

Branching. Ethyl branches are generally produced from reinsertion of in situ generated macromonomers, which are generated from β -H transfer to an ethylene monomer (e.g., Zr–Et group, Scheme 2A). ^{22,54,55} In the present study, ethyl branch density decreases with falling solvent polarity in the \mathbf{Zr}_2 + $\mathbf{B}_{2,n\text{-octyl}}$ -catalyzed ethylene homo- and co-polymerizations (Table 1). The decreased ethyl branch density correlates with the decreased wt % LMW, arguing that the ethyl branches only reside in the LMW product fraction, as confirmed by the ¹³C

Scheme 2. A) Scenario for Ethyl Branch Formation, (B) Competitive Coordination of Monomers and Solvent

A. Ethyl branch formation via chain transfer to monomer

B. Competitive coordination of monomer vs. solvent

$$\begin{array}{c} \bigoplus_{\substack{P' \\ Zr \\ R'}} \stackrel{P'}{ \text{ solvent (solv)}} \\ \end{array} \begin{array}{c} \bigoplus_{\substack{P' \\ Zr \dots | \\ Me \\ Me}} \stackrel{P'}{ } \stackrel{P'}{ } \\ \end{array} \begin{array}{c} \bigoplus_{\substack{P' \\ Zr \dots \text{ solv} \\ Zr \dots \text{ solv} \\ Me \\ Me \\ \end{array}} \begin{array}{c} \bigoplus_{\substack{P' \\ Zr \dots \text{ solv} \\ Zr \dots \text{ solv} \\ Me \\ Me \\ \end{array}}$$

NMR spectral subtraction of the polyethylene samples (Table 2). Note that such analysis is less straightforward for the copolymers, but it is reasonable to assume that the ethyl branch selectivity trend of the same catalyst in ethylene homoand co-polymerizations would be similar.

Regarding n-butyl branch density, it slightly increases with falling solvent polarity in these $\mathbf{Zr_2} + \mathbf{B_{2,n\text{-}octyl}}$ -catalyzed copolymerizations (Table 1). Note that ethylene solubilities in toluene and in MeCy are comparable, so this is not an important variable. More polar/coordinating toluene and toluene/DFB can compete with olefinic monomers for coordination to the cationic Zr center, reasonably accounting for the reduced 1-hexene incorporation in those solvents (Scheme 2B). Note that a similar case was observed when aliphatic solvent-soluble ammonium-based borate cocatalyst was used for olefin polymerizations, in which the in situ formed tertiary amine will coordinate to the cationic metal center and interfere with the catalytic process as well as change the ion-pairing scenario. $^{57-60}$

CONCLUSIONS

Two new binuclear cocatalysts containing alkyl-functionalized trityl cations for homogeneous olefin polymerizations were prepared and characterized, with the structure of $B_{2,t-B_{11}}$ ion pair confirmed by single crystal X-ray diffraction. The newly prepared $B_{2,n\text{-octyl}}$ cocatalyst exhibits good solubility in toluene and aliphatic MeCy solvents, enabling the first implementation of binuclear diborate cocatalysts in low polarity media. In $\mathbf{Zr_2}$ + $B_{2,n\text{-octyl}}$ -catalyzed ethylene homo- and copolymerizations, the catalytic systems respond on changing the solvent from toluene/DFB → toluene → MeCy, with an increase in the wt % HMW fraction in the bimodal product. Concurrently, the ethyl branches, which reside predominantly in LMW fractions of the products, have decreasing densities. However, there is a slight increase in *n*-butyl branch density, which is derived from 1-hexene incorporation in ethylene/1-hexene copolymerization. In parallel, the soluble binuclear diborate cocatalyst was also successfully used in scaled/industrial high temperature, higher pressure olefin polymerizations, demonstrating qualitatively similar solvent effects and comparably broad product

ASSOCIATED CONTENT

Supporting Information

The Supporting Information is available free of charge at https://pubs.acs.org/doi/10.1021/acscatal.2c01676.

Experimental details of cocatalyst synthesis/characterization, crystallographic details (CIF), polymerization experiments, polymer characterization, and details of DFT computation (PDF)

AUTHOR INFORMATION

Corresponding Authors

Tracy L. Lohr — Department of Chemistry, Northwestern University, Evanston, Illinois 60208-3113, United States; Present Address: Shell Global Solutions, Shell Technology Center Houston, 3333 Highway 6 South, Houston, Texas, 77082, United States.; ⊚ orcid.org/0000-0002-4899-2876; Email: tracy.lohr@shell.com

Jerzy Klosin — Corporate R&D, The Dow Chemical Company, Midland, Michigan 48674, United States; orcid.org/0000-0002-9045-7308; Email: jklosin@dow.com

Tobin J. Marks — Department of Chemistry, Northwestern University, Evanston, Illinois 60208-3113, United States; orcid.org/0000-0001-8771-0141; Email: t-marks@northwestern.edu

Authors

Yanshan Gao — Department of Chemistry, Northwestern University, Evanston, Illinois 60208-3113, United States; Present Address: Shanghai Institute of Organic Chemistry, Chinese Academy of Sciences, 345 Lingling Lu, Shanghai 200032, China; orcid.org/0000-0003-0329-705X

Matthew D. Christianson — Corporate R&D, The Dow Chemical Company, Midland, Michigan 48674, United States; © orcid.org/0000-0003-2889-0335

Yang Wang — Department of Chemistry, Northwestern University, Evanston, Illinois 60208-3113, United States Marc P. Coons — Corporate R&D, The Dow Chemical Company, Midland, Michigan 48674, United States; orcid.org/0000-0001-9511-2854

Jiazhen Chen — Department of Chemistry, Northwestern University, Evanston, Illinois 60208-3113, United States; orcid.org/0000-0002-9023-3072

Jialong Zhang — Department of Chemistry, Northwestern University, Evanston, Illinois 60208-3113, United States; Present Address: Shanghai Research Institute of Petrochemical Technology, SINOPEC, 1658 Pudong Beilu, Shanghai, 201208, China.; orcid.org/0000-0002-8205-2204

Steve Marshall – Corporate R&D, The Dow Chemical Company, Midland, Michigan 48674, United States

Complete contact information is available at: https://pubs.acs.org/10.1021/acscatal.2c01676

Notes

The authors declare no competing financial interest.

ACKNOWLEDGMENTS

Financial support by The Dow Chemical Company (Y.G.; Y.W.) is gratefully acknowledged. J.C. and Y.G. were partly supported by the NSF through homogeneous catalysis CAT grant no. CHE-1856619.We thank Drs. E. Carnahan and A. Young of The Dow Chemical Company and C. Carter of Northwestern for helpful discussions and Dr. Y. Zhang for help with NMR experiments. Purchase of the NMR instrumentation

at IMSERC was supported by NIH (1S10OD012016-01/1S10RR019071-01A1). Diffractometry experiments were conducted at IMSERC on Bruker Kappa APEX II instruments purchased with assistance from the State of Illinois and Northwestern University.

REFERENCES

- (1) AlMa'adeed, M. A.-A.; Krupa, I. Polyolefin Compounds and Materials: Fundamentals and Industrial Applications; Springer, 2015.
- (2) Song, F.; Cannon, R. D.; Lancaster, S. J.; Bochmann, M. Activator Effects in Metallocene-Based Alkene Polymerizations: Unexpectedly Strong Dependence of Catalyst Activity on Trityl Concentration. J. Mol. Catal. A: Chem. 2004, 218, 21–28.
- (3) Baier, M. C.; Zuideveld, M. A.; Mecking, S. Post-Metallocenes in the Industrial Production of Polyolefins. *Angew. Chem., Int. Ed.* **2014**, 53, 9722–9744.
- (4) Bochmann, M. The Chemistry of Catalyst Activation: The Case of Group 4 Polymerization Catalysts. *Organometallics* **2010**, *29*, 4711–4740.
- (5) Chen, E. Y.-X.; Marks, T. J. Cocatalysts for Metal-Catalyzed Olefin Polymerization: Activators, Activation Processes, and Structure-Activity Relationships. *Chem. Rev.* **2000**, *100*, 1391–1434.
- (6) McInnis, J. P.; Delferro, M.; Marks, T. J. Multinuclear Group 4 Catalysis: Olefin Polymerization Pathways Modified by Strong Metal-Metal Cooperative Effects. *Acc. Chem. Res.* **2014**, *47*, 2545–2557.
- (7) Delferro, M.; Marks, T. J. Multinuclear Olefin Polymerization Catalysts. *Chem. Rev.* **2011**, *111*, 2450–2485.
- (8) Kaminsky, W. Discovery of Methylaluminoxane as Cocatalyst for Olefin Polymerization. *Macromolecules* **2012**, *45*, 3289–3297.
- (9) Sinn, H.; Kaminsky, W.; Vollmer, H.-J.; Woldt, R. Living Polymers on Polymerization with Extremely Productive Ziegler Catalysts. *Angew. Chem., Int. Ed.* **1980**, *19*, 390–392.
- (10) Chen, E. Y.-X.; Lancaster, S. J. 1.24 Weakly Coordinating Anions: Highly Fluorinated Borates A2. In *Comprehensive Inorganic Chemistry II* (Second ed.); Reedijk, J., Poeppelmeier, K., Eds.; Elsevier, 2013; pp 707-754.
- (11) Yang, X.; Stern, C. L.; Marks, T. J. Cationic Zirconocene Olefin Polymerization Catalysts Based on the Organo-Lewis Acid Tris-(Pentafluorophenyl)Borane—a Synthetic, Structural, Solution Dynamic, and Polymerization Catalytic Study. J. Am. Chem. Soc. 1994, 116, 10015–10031.
- (12) Chien, J. C. W.; Tsai, W. M.; Rausch, M. D. Isospecific Polymerization of Propylene Catalyzed by *rac*-ethylenebis(indenyl)methylzirconium Cation. *J. Am. Chem. Soc.* **1991**, *113*, 8570–8571.
- (13) Kaminsky, W.; Sinn, H. Methylaluminoxane: Key Component for New Polymerization Catalysts. *Adv. Polym. Sci.* **2013**, 258, 1–28.
- (14) Redshaw, C.; Tang, Y. Tridentate ligands and beyond in group IV metal α -olefin homo-/co-polymerization catalysis. *Chem. Soc. Rev.* **2012**, *41*, 4484–4510.
- (15) Makio, H.; Terao, H.; Iwashita, A.; Fujita, T. FI Catalysts for Olefin Polymerization-A Comprehensive Treatment. *Chem. Rev.* **2011**, *111*, 2363–2449.
- (16) Hustad, P. D. Frontiers in Olefin Polymerization: Reinventing the World's Most Common Synthetic Polymers. *Science* **2009**, 325, 704–707.
- (17) Sita, L. R. Ex Uno Plures ("Out of One, Many"): New Paradigms for Expanding the Range of Polyolefins Through Reversible Group Transfers. *Angew. Chem., Int. Ed.* **2009**, *48*, 2464–2472.
- (18) Coates, G. W.; Hustad, P. D.; Reinartz, S. Catalysts for the Living Insertion Polymerization of Alkenes: Access to New Polyolefin Architectures Using Ziegler-Natta Chemistry. *Angew. Chem., Int. Ed.* **2002**, *41*, 2236–2257.
- (19) Gao, Y.; Chen, J.; Wang, Y.; Pickens, D. B.; Motta, A.; Wang, Q. J.; Chung, Y.-W.; Lohr, T. L.; Marks, T. J. Highly Branched Polyethylene Oligomers via Single-Site Polymerization in Very Nonpolar Media. *Nat. Catal.* **2019**, *2*, 236–242.

- (20) Chen, J.; Gao, Y.; Xiong, S.; Delferro, M.; Lohr, T. L.; Marks, T. J. Metal and Counteranion Nuclearity Effects in Organoscandium-Catalyzed Isoprene Polymerization and Copolymerization. *ACS Catal.* **2017**, *7*, 5214–5219.
- (21) Li, H.; Stern, C. L.; Marks, T. J. Significant Proximity and Cocatalyst Effects in Binuclear Catalysis for Olefin Polymerization. *Macromolecules* **2005**, *38*, 9015–9027.
- (22) Li, L.; Metz, M. V.; Li, H.; Chen, M.-C.; Marks, T. J.; Liable-Sands, L.; Rheingold, A. L. Catalyst/Cocatalyst Nuclearity Effects in Single-Site Polymerization. Enhanced Polyethylene Branching and α -Olefin Comonomer Enchainment in Polymerizations Mediated by Binuclear Catalysts and Cocatalysts via a New Enchainment Pathway. *J. Am. Chem. Soc.* **2002**, *124*, 12725–12741.
- (23) Motolko, K. S. A.; Price, J. S.; Emslie, D. J. H.; Jenkins, H. A.; Britten, J. F. Zirconium Complexes of a Rigid, Dianionic Pincer Ligand: Alkyl Cations, Arene Coordination, and Ethylene Polymerization. *Organometallics* **2017**, *36*, 3084–3093.
- (24) Gu, W.; Stalzer, M. M.; Nicholas, C. P.; Bhattacharyya, A.; Motta, A.; Gallagher, J. R.; Zhang, G.; Miller, J. T.; Kobayashi, T.; Pruski, M.; et al. Benzene Selectivity in Competitive Arene Hydrogenation: Effects of Single-Site Catalyst···Acidic Oxide Surface Binding Geometry. *J. Am. Chem. Soc.* **2015**, *137*, 6770–6780.
- (25) Gillis, D. J.; Quyoum, R.; Tudoret, M.-J.; Wang, Q.; Jeremic, D.; Roszak, A. W.; Baird, M. C. Synthesis and Characterization of the Series of d⁰ Arene Complexes $[Cp*MMe_2(\eta^6\text{-arene})][MeB(C_6F_5)_3]$ (M = Ti, Zr, Hf). Organometallics 1996, 15, 3600–3605.
- (26) Lehmann, M.; Schulz, A.; Villinger, A. Bissilylated Halonium Ions: $[Me_3Si-X-SiMe_3][B(C_6F_5)_4]$ (X = F, Cl, Br, I). *Angew. Chem., Int. Ed.* **2009**, 48, 7444–7447.
- (27) Stahl, N. G.; Salata, M. R.; Marks, T. J. $B(C_6F_5)_3$ vs $Al(C_6F_5)_3$ -Derived Metallocenium Ion Pairs. Structural, Thermochemical, and Structural Dynamic Divergences. *J. Am. Chem. Soc.* **2005**, 127, 10898–10909.
- (28) Zaccaria, F.; Sian, L.; Zuccaccia, C.; Macchioni, A. Chapter One-Ion Pairing in Transition Metal Catalyzed Olefin Polymerization. In *Advances in Organometallic Chemistry*; Pérez, P. J., Ed.; Academic Press, 2020; Vol. 73, pp 1–78.
- (29) Sian, L.; Macchioni, A.; Zuccaccia, C. Understanding the Role of Metallocenium Ion-Pair Aggregates on the Rate of Olefin Insertion into the Metal—Carbon Bond. ACS Catal. 2020, 10, 1591–1606.
- (30) Zimmer, K. D.; Shoemaker, R.; Ruminski, R. R. Synthesis and Characterization of a Fluxional Re(I) Carbonyl Complex *fac*[Re(CO)₃(dpop')Cl] with the Nominally Tri-dentate Ligand Dipyrido(2,3-a:3',2'-j)phenazine (dpop'). *Inorg. Chim. Acta* **2006**, 359, 1478–1484.
- (31) Carrión, M. C.; Guerrero, A.; Jalón, F. A.; Manzano, B. R.; De La Hoz, A.; Claramunt, R. M.; Milata, V.; Elguero, J. Five Different Fluxional Processes in Polyfluorophenyl Palladium(II) Complexes with 2,4,6-tris(3,5-dimethylpyrazol-1-yl)-1,3,5-triazine. The Driving Effect of the Solvent. *Inorg. Chem.* **2003**, *42*, 885–895.
- (32) Bellachioma, G.; Ciancaleoni, G.; Zuccaccia, C.; Zuccaccia, D.; Macchioni, A. NMR Investigation of Non-Covalent Aggregation of Coordination Compounds Ranging from Dimers and Ion Pairs up to Nano-Aggregates. *Coord. Chem. Rev.* **2008**, 252, 2224–2238.
- (33) Zuccaccia, C.; Stahl, N. G.; Macchioni, A.; Chen, M.-C.; Roberts, J. A.; Marks, T. J. NOE and PGSE NMR Spectroscopic Studies of Solution Structure and Aggregation in Metallocenium Ion-Pairs. *J. Am. Chem. Soc.* **2004**, *126*, 1448–1464.
- (34) Stahl, N. G.; Zuccaccia, C.; Jensen, T. R.; Marks, T. J. Metallocene Polymerization Catalyst Ion-Pair Aggregation by Cryoscopy and Pulsed Field Gradient Spin-Echo NMR Diffusion Measurements. J. Am. Chem. Soc. 2003, 125, 5256–5257.
- (35) Chai, J.-D.; Head-Gordon, M. Systematic Optimization of Long-Range Corrected Hybrid Density Functionals. *J. Chem. Phys.* **2008**, *128*, 084106.
- (36) Chai, J.-D.; Head-Gordon, M. Long-Range Corrected Hybrid Density Functionals with Damped Atom-Atom Dispersion Corrections. *Phys. Chem. Chem. Phys.* **2008**, *10*, 6615–6620.

- (37) Hustad, P. D.; Kuhlman, R. L.; Arriola, D. J.; Carnahan, E. M.; Wenzel, T. T. Continuous Production of Ethylene-based Diblock Copolymers using Coordinative Chain Transfer Polymerization. *Macromolecules* **2007**, *40*, 7061–7064.
- (38) Gao, Y.; Christianson, M. D.; Wang, Y.; Chen, J.; Marshall, S.; Klosin, J.; Lohr, T. L.; Marks, T. J. Unexpected Precatalyst σ-Ligand Effects in Phenoxyimine Zr-Catalyzed Ethylene/1-Octene Copolymerizations. *J. Am. Chem. Soc.* **2019**, *141*, 7822–7830.
- (39) Gao, Y.; Chen, X.; Zhang, J.; Chen, J.; Lohr, T. L.; Marks, T. J. Catalyst Nuclearity Effects on Stereo- and Regionduction in Pyridylamidohafnium-Catalyzed Propylene and 1-Octene Polymerizations. *Macromolecules* **2018**, *51*, 2401–2410.
- (40) Li, H.; Li, L.; Marks, T. J. Polynuclear Olefin Polymerization Catalysis: Proximity and Cocatalyst Effects Lead to Significantly Increased Polyethylene Molecular Weight and Comonomer Enchainment Levels. *Angew. Chem., Int. Ed.* **2004**, 43, 4937–4940.
- (41) Jung, M.; Lee, Y.; Kwak, S.; Park, H.; Kim, B.; Kim, S.; Lee, K. H.; Cho, H. S.; Hwang, K. Y. Analysis of Chain Branch of Polyolefins by a New Proton NMR Approach. *Anal. Chem.* **2016**, *88*, 1516–1520.
- (42) Galland, G. B.; de Souza, R. F.; Mauler, R. S.; Nunes, F. F. 13 C NMR Determination of the Composition of Linear Low-Density Polyethylene Obtained with $[\eta^3$ -Methallyl-nickel-diimine]PF₆ Complex. *Macromolecules* **1999**, 32, 1620–1625.
- (43) Li, H.; Li, L.; Marks, T. J.; Liable-Sands, L.; Rheingold, A. L. Catalyst/Cocatalyst Nuclearity Effects in Single-Site Olefin Polymerization. Significantly Enhanced 1-Octene and Isobutene Comonomer Enchainment in Ethylene Polymerizations Mediated by Binuclear Catalysts and Cocatalysts. J. Am. Chem. Soc. 2003, 125, 10788–10789.
- (44) Schiebel, E.; Voccia, M.; Falivene, L.; Caporaso, L.; Mecking, S. The Impact of Charge in a Ni(II) Polymerization Catalyst. *ACS Catal.* **2021**, *11*, 5358–5368.
- (45) Sifri, R. J.; Padilla-Vélez, O.; Coates, G. W.; Fors, B. P. Controlling the Shape of Molecular Weight Distributions in Coordination Polymerization and Its Impact on Physical Properties. *J. Am. Chem. Soc.* **2020**, *142*, 1443–1448.
- (46) Zou, C.; Dai, S.; Chen, C. Ethylene Polymerization and Copolymerization Using Nickel 2-Iminopyridine-N-oxide Catalysts: Modulation of Polymer Molecular Weights and Molecular-Weight Distributions. *Macromolecules* **2018**, *51*, 49–56.
- (47) Stürzel, M.; Mihan, S.; Mülhaupt, R. From Multisite Polymerization Catalysis to Sustainable Materials and All-Polyolefin Composites. *Chem. Rev.* **2016**, *116*, 1398–1433.
- (48) Agapie, T.; Henling, L. M.; DiPasquale, A. G.; Rheingold, A. L.; Bercaw, J. E. Zirconium and Titanium Complexes Supported by Tridentate LX2 Ligands Having Two Phenolates Linked to Furan, Thiophene, and Pyridine Donors: Precatalysts for Propylene Polymerization and Oligomerization. *Organometallics* 2008, 27, 6245–6256.
- (49) Roberts, J. A. S.; Chen, M.-C.; Seyam, A. M.; Li, L.; Zuccaccia, C.; Stahl, N. G.; Marks, T. J. Diverse Stereocontrol Effects Induced by Weakly Coordinating Anions. Stereospecific Olefin Polymerization Pathways at Archetypal Cs- and C1-Symmetric Metallocenium Catalysts Using Mono- and Polynuclear Halo-perfluoroarylmetalates as Cocatalysts. J. Am. Chem. Soc. 2007, 129, 12713—12733.
- (50) Chen, M.-C.; Roberts, J. A. S.; Seyam, A. M.; Li, L.; Zuccaccia, C.; Stahl, N. G.; Marks, T. J. Diversity in weakly coordinating anions. Mono- and polynuclear halo(perfluoroaryl)metalates as cocatalysts for stereospecific olefin polymerization: Synthesis, structure, and reactivity. *Organometallics* **2006**, *25*, 2833–2850.
- (51) Chen, M.-C.; Roberts, J. A. S.; Marks, T. J. New mononuclear and polynuclear perfluoroarylmetatate cocatalysts for stereospecific olefin polymerization. *Organometallics* **2004**, *23*, 932–935.
- (52) Gunasekara, T.; Kim, J.; Xiong, S.; Preston, A.; Steelman, D. K.; Medvedev, G. A.; Delgass, W. N.; Caruthers, J. M.; Abu-Omar, M. M. Interaction between Two Active Sites of the Same Catalyst for Macromonomer Enchained Olefin Polymerization. *Macromolecules* **2017**, *50*, 9151–9161.
- (53) Liu, S.; Invergo, A. M.; McInnis, J. P.; Mouat, A. R.; Motta, A.; Lohr, T. L.; Delferro, M.; Marks, T. J. Distinctive Stereochemically

- Linked Cooperative Effects in Bimetallic Titanium Olefin Polymerization Catalysts. *Organometallics* **2017**, *36*, 4403–4421.
- (54) Li, H.; Marks, T. J. Nuclearity and Cooperativity Effects in Binuclear Catalysts and Cocatalysts for Olefin Polymerization. *Proc. Natl. Acad. Sci. U.S.A.* **2006**, *103*, 15295–15302.
- (55) Izzo, L.; Caporaso, L.; Senatore, G.; Oliva, L. Branched Polyethylene by Ethylene Homopolymerization with *meso-*Zirconocene Catalyst. *Macromolecules* **1999**, 32, 6913–6916.
- (56) Hayduk, W. IUPAC Solubility Data Series: Ethene; Oxford University Press, 1994.
- (57) Rocchigiani, L.; Ciancaleoni, G.; Zuccaccia, C.; Macchioni, A. An Integrated NMR and DFT Study on the Single Insertion of α -Olefins into the M C Bond of Group 4 Metallaaziridinium Ion Pairs. *ChemCatChem* **2013**, *5*, 519–528.
- (58) Rocchigiani, L.; Ciancaleoni, G.; Zuccaccia, C.; Macchioni, A. Low-Temperature Kinetic NMR Studies on the Insertion of a Single Olefin Molecule into a Zr-C Bond: Assessing the Counterion-Solvent Interplay. *Angew. Chem., Int. Ed.* **2011**, *50*, 11752–11755.
- (59) Rocchigiani, L.; Bellachioma, G.; Ciancaleoni, G.; Macchioni, A.; Zuccaccia, D.; Zuccaccia, C. Synthesis, Characterization, Interionic Structure, and Self-Aggregation Tendency of Zirconaaziridinium Salts Bearing Long Alkyl Chains. *Organometallics* **2011**, *30*, 100–114.
- (60) Rocchigiani, L.; Zuccaccia, C.; Zuccaccia, D.; Macchioni, A. Self-Aggregation Tendency of Zirconocenium Ion Pairs Which Model Polymer-Chain-Carrying Species in Aromatic and Aliphatic Solvents with Low Polarity. *Chem.—Eur. J.* **2008**, *14*, 6589–6592.

TRecommended by ACS

Diborative Reduction of Alkynes to 1,2-Diboryl-1,2-Dimetalloalkanes: Its Application for the Synthesis of Diverse 1,2-Bis(boronate)s

Fumiya Takahashi, Hideki Yorimitsu, et al.

JUNE 12, 2019 ORGANIC LETTERS

READ 🖸

Triarylborane-Catalyzed Formation of Cyclic Organic Carbonates and Polycarbonates

Kori A. Andrea and Francesca M. Kerton

JANUARY 17, 2019 ACS CATALYSIS

READ 🗹

Suzuki-Miyaura Coupling of Simple Ketones via Activation of Unstrained Carbon-Carbon Bonds

Ying Xia, Guangbin Dong, et al.

APRIL 13, 2018

JOURNAL OF THE AMERICAN CHEMICAL SOCIETY

READ 🗹

BArF3-Catalyzed Imine Hydroboration with Pinacolborane Not Requiring the Assistance of an Additional Lewis Base

Qin Yin, Martin Oestreich, et al.

JUNE 19, 2017

ORGANOMETALLICS

READ 🗹

Get More Suggestions >